ELSEVIER

International Journal of Heat and Fluid Flow 22 (2001) 308–314

International Journal of
HEAT AND
FLUID FLOW

www.elsevier.com/locate/ijhff

Flow and heat transfer in a rotating U-bend with 45° ribs

H. Iacovides, D.C. Jackson, G. Kelemenis, B.E. Launder *, Y.-M. Yuan

Department of Mechanical Engineering, UMIST, P.O. Box 88, Manchester M60 IQD, UK

Abstract

Velocity and heat transfer measurements are reported of flow through a square-ended U-bend with 45° ribs rotating in orthogonal mode. The configuration provides an idealization of the flow within modern cooled gas-turbine blades to provide data against which predictions of CFD methods for such industrial configurations can be rigorously tested. The U-bend was mounted on a rotating table with water as working fluid. The heat-transfer data were obtained at a Reynolds number of 36,000 with rotation numbers of 0.1 and 0.2 as well as for a stationary duct. The angled ribs generate streamwise vortices which, together with the enhanced mixing induced by the ribs, means that the flow and average Nusselt numbers are relatively unaffected by rotation. However, rotation does lead to local hot – or cold – spots which in an actual blade would mean large temperature gradients with consequent stress concentrations.

1. Introduction

The present experimental contribution is aimed at providing as complete a documentation as possible of a duct flow configuration that reproduced the essential features found in the internal cooling passages of a modern gas-turbine blade. A square-ended rotating U-bend, roughened with square-sectioned ribs aligned at 45° with the duct axis, has been chosen for study. As has been established in previous investigations, the orientation of the ribs partly in the flow direction leads to the creation of appreciable streamwise vorticity which modifies the flow and the consequent distribution of heat transfer coefficient (e.g., Lau et al., 1991; Han and Zhang, 1992; Taslim et al., 1996). In an actual blade cooling passage secondary flows are also created by Coriolis forces arising from blade rotation and by the successive passage of the flow around the abrupt U-bends in the serpentine cooling channel. There are, in addition, the effects of Coriolis forces directly on the turbulent stresses which tend to suppress fluctuations normal to the wall near the suction surface while augmenting them close to the pressure surface, e.g., Kasagi (1998). In combination these agencies create one of the most complex strain fields arising in single-phase flow. While previous studies have examined the effects of rib roughness, rotation and the U-bends (usually) on the mean heat transfer, the simultaneous measurement of local heat transfer coefficient and the velocity field in the present study is aimed at providing a more complete basis to understand physically what is happening in the cooling passage and to provide a more searching test for any CFD code.

Like our earlier studies, the present experiments have used water as the working fluid and thus do not include the additional "buoyant" effects from the rotation of hot (and appreciably less dense) near wall fluid that occurs in an actual blade. It is no bad thing to separate these effects to distinguish between flow complexities associated with the highly three-dimensional strain field from those due to buoyancy. An earlier CFD study by Bo et al. (1995) of the smooth rotating duct data of Wagner et al. (1989) suggested that these buoyant effects – which were substantial at least in the smooth-walled channel considered – were satisfactorily accounted for with conventional modelling.

2. Apparatus and instrumentation

The present experiments were undertaken in the rotating water-loop facility, previously described in earlier papers from the group (e.g., Cheah et al., 1996). Briefly, a horizontal rotating motor-driven table is mounted within a stationary 1.22 m diameter tank. Water is circulated in a closed-loop system being first metered in a straight section containing an orifice plate before arriving through a vertical pipe at the centre of the rotating table whence it enters an internal passage through which it is ducted to the U-bend, Fig. 1. The duct cross section is 50 mm square with the two walls parallel to the rotation axis being roughened with 5.0 mm square ribs spaced 50 mm apart and oriented at 45° with the duct axis. Velocity-field data were obtained by LDA employing a stationary fibre-optic probe mounted above the rotating section, as described in Cheah et al. (1996), and by video-recorded flow visualization where the camera and illumination system rotate with the duct. In the course of the present work the capability of the apparatus has been extended to provide local surface heat transfer measurements, in the rotating duct, Kelemenis (1999) and Iacovides et al. (1999). The arrangement is shown schematically in Fig. 2. Power is supplied to the table through slip rings. The power required to raise the wall temperature 10°C above the bulk

* Corresponding author. Tel.: +44-161-200-3701; fax: +44-161-200-3723.

E-mail address: brian.launder@umist.ac.uk (B.E. Launder).

0142-727X/01/$ - see front matter
PII: S0142-727X(01)00093-5

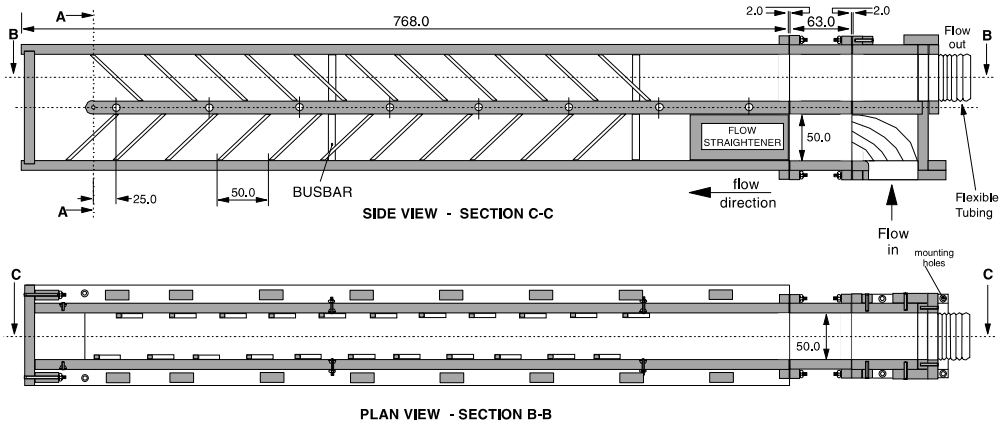

Fig. 1. Experimental model of square-ended ribbed U-bend.

fluid temperature (80 kW/m^2) necessitated heating (just) the ribbed side walls in four separate sections on each side as shown. There were breaks in the heating due to bus-bars and along a narrow strip at the U-bend itself. These appear in the Nusselt number results as blank sections on the diagrams.

The liquid crystals used for temperature measurements, although ''encapsulated'', proved to be seriously affected by water. Accordingly, a liquid crystal coating was sprayed directly onto the Perspex side walls which was then covered by black ink, then the stainless steel foil was affixed with double-sided adhesive tape. The colour play of the liquid crystals was viewed externally through the Perspex walls. The copper ribs were affixed directly to the heating foil with a thin film of Araldite which provided sufficient electrical resistance to isolate the ribs but negligible thermal resistance. The ribs thus effectively reached an isothermal state, their temperature being the level required to cause convective heat transfer to the passing water at the same rate as heat entered via the surface in contact with the foil. For further details the reader is referred to Kelemenis (1999). The liquid crystal images were recorded on a video camera, each image covering a patch approximately 100 mm square. At each location five to six images were recorded, corresponding to thermally steady-state conditions at different heating rates. The camera position was then successively moved until the whole duct had been covered. The images were subsequently digitised and, through software developed during the course of these investigations, the pixels with a hue number corresponding to the yellow colour, and hence a known temperature, were identified. Knowledge of the wall heat flux rate, from the electrical power measurements, and of the local bulk temperature, from an energy balance, enabled us to calculate the local Nusselt number along constant colour contours. By combining information from different heating rates a full mapping of the local Nusselt number over the heated surfaces was produced.

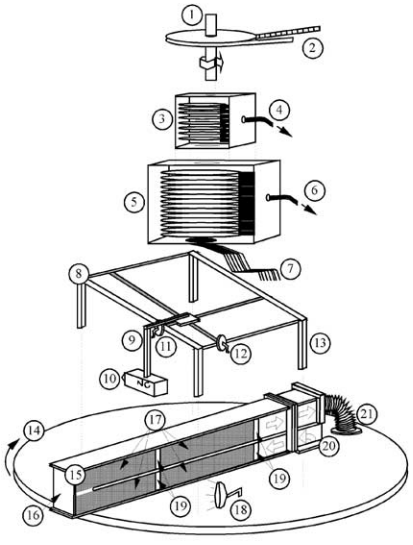

Fig. 2. Rotating flow rig: (1) rotating shaft; (2) toothbelt; (3) signal sliprings; (4) data output; (5) power sliprings; (6) power input; (7) power cables; (8) traversing gear; (9) camera arm; (10) video camera; (11) lengthwise adjustment; (12) crosswise adjustment; (13) pillar supports; (14) turntable; (15) model (square-ended duct); (16) bridging (brass) plate; (17) foil covered sections; (18) illumination; (19) busbars; (20) flow-feed tower; (21) flexible exhaust hose.

3. Presentation of the results

An essential to understanding the surface heat-transfer pattern in a given configuration is to know the nature of the velocity field in the vicinity of the surface. Thus we consider first information gathered about the mean velocity before examining the resultant local heat-transfer behaviour. In the present paper we report first the qualitative results of flow visualization studies and then present the available LDA measurements of the mean velocity field. Flow conditions are characterised by two dimensionless numbers, the flow Reynolds number, Re and the rotation number, Ro. They are defined as

$$Re \equiv U_B D/\nu \quad \text{and} \quad Ro \equiv \Omega D/U_B,$$

where U_B is the fluid bulk velocity, D the duct hydraulic diameter and Ω the angular velocity of the rotating U-bend.

The 45° orientation of the ribs leads to the creation of a strong streamwise vortex shed from the downstream side of each rib which then merges with those shed from ribs further upstream, Fig. 3. The vortices shed from the two ribbed walls, with an opposite sign of vorticity, are symmetrically placed with respect to the duct centre-plane in the case of no rotation (Fig. 3(a)). When rotation is present ($R_0 = +0.1$), Fig. 3(b), the Coriolis-induced secondary flow displaces the vortices towards the leading (suction) side of the duct. This shift, while small, has an important effect on the flow structure in the turn region.

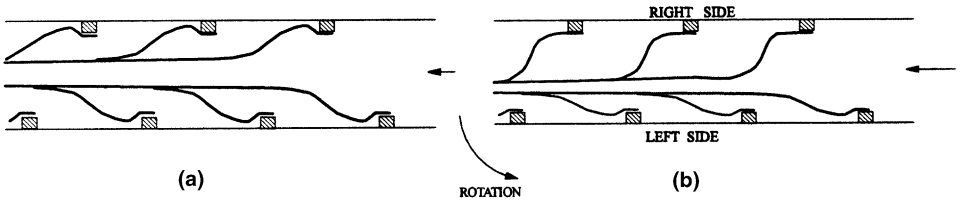

Fig. 3. Plan view of flow-visualisation traces of rib-generated vortices in upstream section: (a) stationary case; (b) rotating case $Ro = +0.1$.

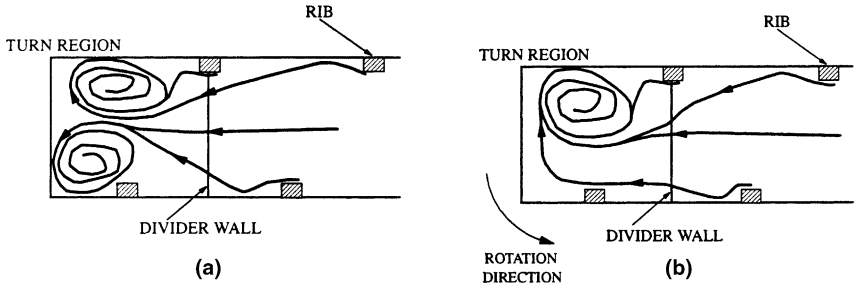

Fig. 4. Plan view of flow-visualisation traces of rib-generated vortices within the bend: (a) stationary case; (b) rotating case $Ro = +0.1$.

As is seen from Fig. 4, with no rotation two distinct, nearly symmetric1 [1] vortices roll up. With duct rotation, however, the vortices originating from the two sides (with opposite signs of vorticity) wrap up around each other leading to just a single consolidated vortex passing around the U-bend. One possible explanation is that, as the flow turns from a direction normal to one parallel to the axis of rotation, the Coriolis force disappears and at the bend entry a favourable pressure gradient develops along the trailing side and an adverse one along the leading side. This would intensify the vortex generated along the trailing side and dilute that generated along the leading side, leading to the single vortex observed in the bend. We note that, contrary to what might be expected, for $R_0 = +0.1$, the vortex centre is located near the trailing wall at entry to the U-bend. Fig. 5 finally provides a view of the U-bend region as viewed through the ribbed walls. Again heavy solid lines indicate the path of the vortex while the broken lines indicate approximately the paths followed by air bubbles released from the vortex. For the flow upstream of the turn, the rib-induced vortex is now seen to originate at the upstream root of the rib and to run parallel with the rib along most of its length, especially in the case of positive rotation along the pressure side (due to the Coriolis-induced secondary motion). We note too the expected recirculating eddies in the upper and lower corners of the turn, as well as the recirculation zone of the inner wall immediately downstream of the bend. Downstream of the turn, the visible lengths of the vortices shed from the ribs are evidently shorter, suggesting more rapid diffusion.

Fig. 6 shows the available LDA measurements of the mean flow field for the stationary case. The data are presented in the form of vector plots along three planes normal to the ribbed walls; a plane near, at a distance of 9% of the duct diameter, the inner (smooth) wall, the mid-plane and a plane near the outer (smooth) wall, also at a distance of 9% of the duct diameter. It should be noted that LDA measurements have been obtained at a Reynolds number of 100,000, while the subsequent heat transfer measurements at a Reynolds number of 36,000. The reduction in Reynolds number for the heat transfer tests became necessary because of the high heating rates needed to maintain an acceptable difference between the wall and the fluid temperatures (about 10 K). In the straight section before the bend the measurements show that along the

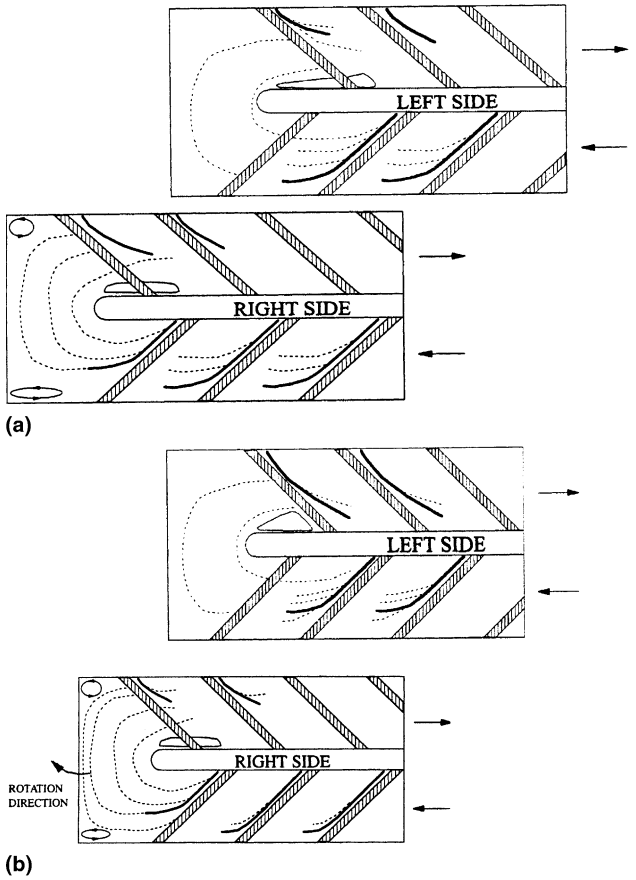

Fig. 5. Side view of flow-visualisation traces of rib-generated vortices: (a) stationary case; (b) rotating case $Ro = +0.1$.

[1] Due to the staggered ribs a completely symmetric pattern would not be expected.

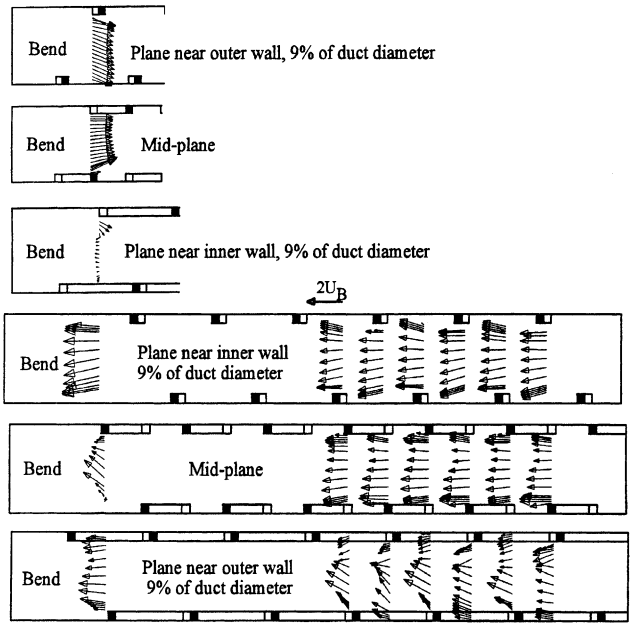

Fig. 6. Measured mean velocity field along planes normal to the ribbed walls, for a stationary U-bend at $Re = 100{,}000$.

inner wall the fluid spreads from the duct centre towards the ribbed walls, while along the outer wall the opposite trend is observed. This is consistent with the presence of rib-induced secondary motion, reported in a parallel numerical study by Raisee (1999), from which a representative plot is reproduced in Fig. 7. This rib-induced secondary motion also explains why, as shown by the flow visualisation results of Fig. 5, the rib-induced vortex generated at the upstream root of each rib, along the inner wall, does not extend all the way to the downstream root, along the outer wall. Near the outer wall, the cross-duct motion from the ribbed walls to the duct centre, turns the rib-induced vortex in a direction parallel to that of

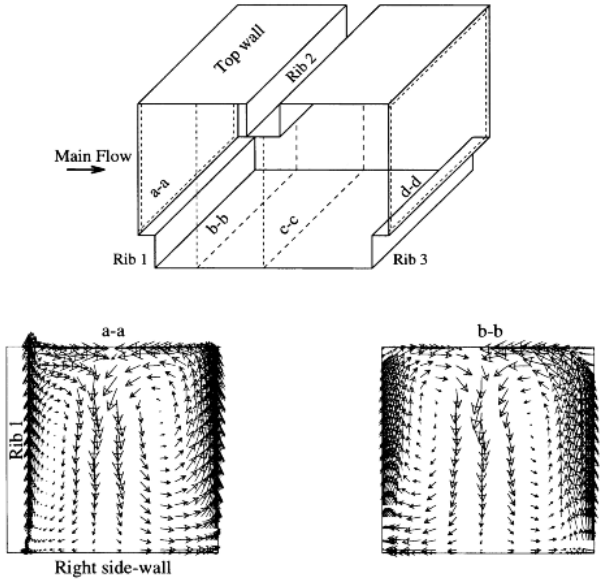

Fig. 7. Computed rib-induced secondary motion (Raisee, 1999) along planes parallel to the inclined ribs, for repeating flow in a straight duct with 45° ribs.

the main flow. At the bend entry, the LDA data of Fig. 6 show that the flow along the inner wall is accelerated. This is also seen in smooth U-bends and it is caused by the strong favourable pressure gradient. Contrary to what is observed in smooth U-bends, no corresponding flow deceleration is shown by the LDA data along the outer wall, at the bend entry. This may be a result of the rib-induced secondary motion that transports fluid from the inner to the outer wall. Along the mid-plane, at the bend entry, the strong rib-induced vortex along the right side, also seen in the flow visualisation results in Fig. 4, is again evident. At the exit plane, along the inner wall there is a large separation bubble over most of the duct diameter apart from a region close to the left side. This feature is again consistent with the flow visualisation tests that suggest that along this side flow separation occurs after the bend exit. At the mid- and outer-wall planes the streamwise velocity component is fairly uniform, while the direction of the cross-duct motion is determined by the presence of ribs along the right and left sides respectively.

Fig. 8 shows the corresponding LDA measurements under rotating conditions, at a rotation number of −0.1. In the upstream section, along the two smooth walls there is a change in the cross-duct motion, which is now directed towards the leading ribbed side, while along the mid-plane the opposite change is noticeable. Both these changes are consistent with the presence of the Coriolis-driven secondary motion. At the bend entry the fluid along the outer wall is now slowed down, while along the mid-plane it is markedly faster, in comparison to the stationary case. Both these changes could be due to the

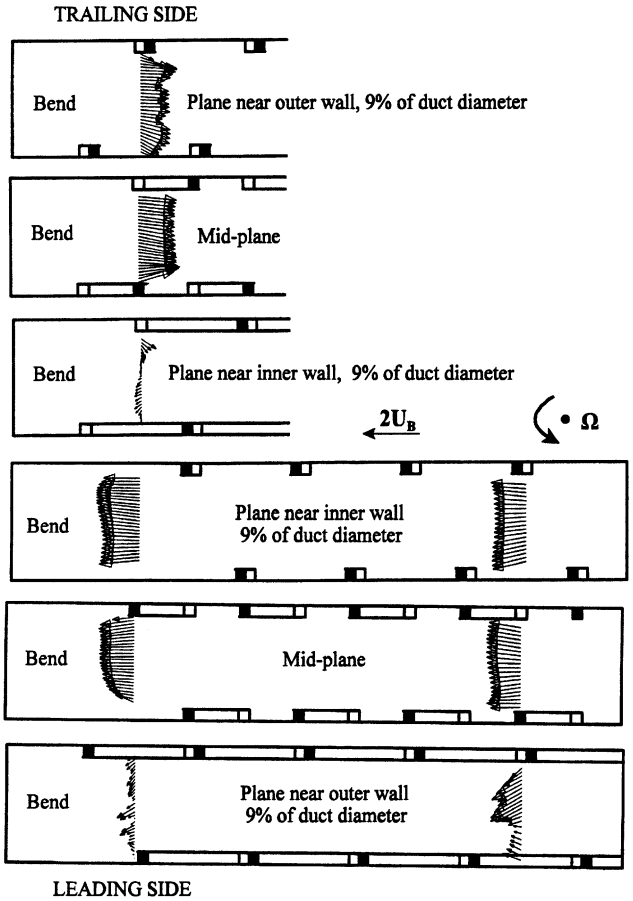

Fig. 8. Measured mean velocity field along planes normal to the ribbed walls, for a stationary U-bend at $Re = 100{,}000$ and $Ro = -0.1$.

fact that the Coriolis-induced secondary motion, inhibits the rib-induced secondary motion, thus diminishing the transport of fluid towards the outer side. At the bend exit, the strongest differences between the rotating and stationary case appear to be along the outer wall, where rotation appears to result in a more non-uniform distribution of the streamwise flow, with slower motion along the leading side.

The LDA measurements are thus consistent with the flow visualisation data. They suggest that heat transfer levels should be high after the upstream root of each rib and lower near the downstream root. At the bend entry the flow data also suggest that if the upstream root of the last rib is as close as half a diameter from the bend entry (left side), heat transfer levels, along that side will be lower. The effects of rotation are rather harder to infer from the available flow-field data. Upstream of the bend heat transfer levels along the trailing side are expected to be higher than those along the leading side.

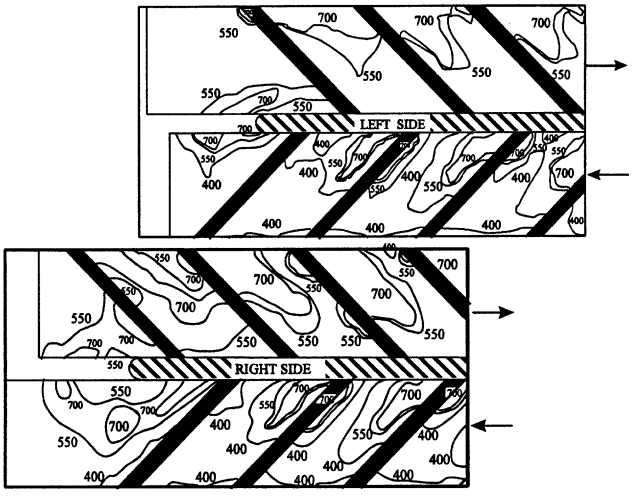

Fig. 9. Nusselt number contours for a stationary ribbed U-bend, at $Re = 36{,}000$ and $Pr = 5.9$.

Attention is now turned to the local heat transfer coefficient. As has been mentioned this excludes the ribs themselves and the region where the bus bars are affixed. Contour plots of Nusselt number are shown in Figs. 9–12, while Kelemenis (1999) provides a coloured mapping which permits a more detailed resolution to be drawn. First, Fig. 9, for the stationary duct, upstream of the bend one notes a repeating pattern, essentially the same on each side of the duct with the peak Nusselt number arising near the upstream root of the ribs with the contours aligning with the rib-induced vortex discussed earlier. Compared with the data of Taslim et al. (1996), the peak Nusselt numbers are closer to the root of the rib. The variation in their experiments between the maximum and minimum Nusselt number was more than 6:1 for $e/D = 0.125$ compared to 2.5:1 in the present case. ($e/D = 0.1$). In the present experiments only the two ribbed walls were heated and the fluid was water rather than air. Superficially, however, these differences would seem likely to produce *larger* local variations in *Nu*.

Downstream from the final rib preceding the turn, the symmetry of the *Nu* pattern on the two sides of the duct disappears. The turning of the vortex on the right side leaves a very clear imprint on the heat transfer coefficient. Downstream of the bend, a broadly similar pattern of heat transfer to that upstream of the bend is gradually re-established but the levels of *Nu* are higher and are now different on the two sides, at least over the first six rib intervals to which our measurements have been confined.

Fig. 10 shows the corresponding pattern in the case of rotation ($R_0 = 0.1$). There has clearly been a considerable change upstream of the bend with higher Nusselt numbers near the origin of the rib-induced vortex on the upstream end of the ribs but lower levels in islands mid-way between ribs of the right side, which, in the upstream section, is the pressure side. Along the left side, the size of the high *Nu* region after each rib is markedly reduced. The rotation effects on heat transfer along the left side of the upstream section are certainly consistent with the expected effects of the Coriolis-driven secondary motion, which lead to an accumulation of slower fluid on the suction side of the rotating duct. Along the right side of the

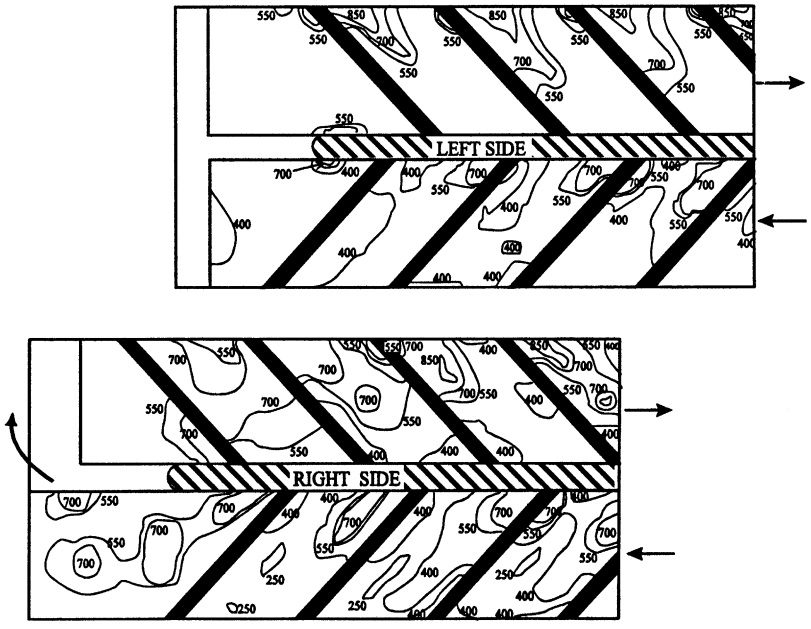

Fig. 10. Nusselt number contours for a rotating ribbed U-bend, at $Ro = +0.1$, $Re = 36{,}000$ and $Pr = 5.9$.

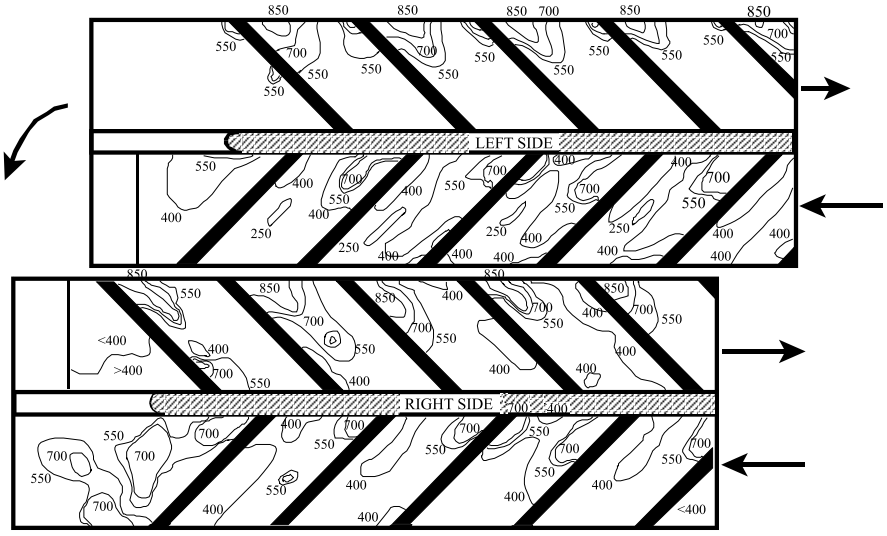

Fig. 11. Nusselt number contours for a rotating ribbed U-bend, at $Ro = -0.1$, $Re = 36{,}000$ and $Pr = 5.9$.

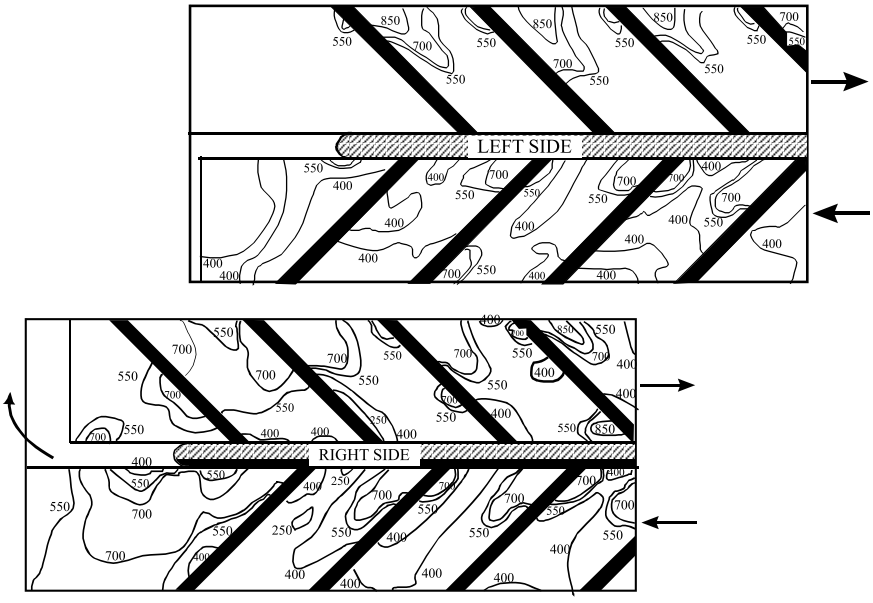

Fig. 12. Nusselt number contours for a rotating ribbed U-bend, at $Ro = +0.2$, $Re = 36{,}000$ and $Pr = 5.9$.

upstream section, the fact that, as shown by the flow visualisation data, the vortex generated downstream of each rib is strengthened by rotation, is consistent with the greater variation in local Nusselt number observed within each rib interval. As can be seen in Fig. 11, the test was repeated with the direction of rotation reversed and all the same features were retained, only transposed from the left to the right side. In the turn region itself there is, as for the non-rotating case, a strong peak in Nusselt number immediately downstream of the last rib on the right side (indeed peak levels higher than $R_0 = 0$). There is no clear imprint of a collective rib-induced vortex as it undergoes the 180° turn however, possibly because its strength is diminished by the vortex threads of opposite sign becoming wrapped together. Downstream of the bend along the left side (now the high pressure side), while peak levels are higher than for the stationary case, they are confined to a narrower region close to the upstream root of the each rib. Along the right side on the other hand (which, downstream of the bend, becomes the suction side), positive rotation causes the high Nusselt number regions within each interval to contract. These effects of rotation on the downstream thermal development are similarly linked to the effects of rotation on the flow development, as those in the upstream section discussed earlier. Reversing the direction of rotation, Fig. 11, causes two distinct high Nusselt number regions to appear along the right side of the turn region. The first starts at the upstream root of the last rib and is aligned parallel to it. It is clearly caused by the rib-induced vortex. The second starts at the downstream root of the last rib and is aligned in a direction normal to it. Lack of flow data over this part of the bend makes it difficult to speculate on probable causes. Downstream of the bend, along the left side, peak Nusselt number levels are also higher than for the stationary case, but are confined to an even shorter region within each rib interval than for the case of positive rotation. On the

right side, which downstream of the bend becomes the high-pressure side, peak Nusselt number levels are higher than for either the stationary case or the case of positive rotation, but are confined to a narrower region within the upstream half of each rib interval.

Increasing the rotation number to 0.2, Fig. 12, has the surprising effect of producing a patch of high *Nu* on the left side upstream of the penultimate rib before the turn. Again the duct rotation was reversed and the high *Nu* patch appeared in the corresponding position on the opposite wall. Unfortunately, no dynamic field data have been obtained at this rotation number that might throw light on the reason for this local peak.

4. Concluding remarks

Local Nusselt numbers have been reported for flow through a square-ended U-bend roughened by square-sectioned ribs aligned at 45° with the flow direction, a configuration representative of those currently in use or under development for blade-cooling passages. The heat-transfer data have been augmented by flow visualisation and LDA studies. The effect of the ribs on the heat transfer is to more than double the Nusselt number compared with our earlier data for a smooth duct. However, the augmentation is far from uniform with the highest heat transfer arising beneath the intense vortex originating from the upstream root of the ribs. The imprint of this can also be clearly seen on the right side as it tracks around the U-bend. The main effect of rotation on the heat transfer is that, while the average level of Nusselt number is not greatly affected, higher and lower levels are recorded in particular regions, a result which may have significant implications for the level of thermal stresses induced.

Acknowledgements

The research was sponsored by ABB, EGT and Electricité de France and is published by permission. Expert technical assistance was provided by Mr. D. Cooper and Mr M. Jackson. Authors' names are listed alphabetically.

References

Bo, T., Iacovides, H., Launder, B.E., 1995. ASME J. Turbomachinery 117, 474–484.

Cheah, S.C., Iacovides, H., Jackson, D.C., Ji, H., Launder, B.E., 1996. ASME J. Turbomachinery 118, 590–596.

Han, J.C., Zhang, Y.M., 1992. ASME J. Heat Transfer 114, 850–858.

Iacovides, H., Jackson, D.C., Kelemenis, G., Launder, B.E., Yuan, Y.-M., 1999. Int. J. Heat Fluid Flow 20, 302–311.

Kasagi, N., 1998. Progress in direct numerical simulation of turbulent transport and its control. Int. J. Heat Fluid Flow 19, 125–134.

Kelemenis, G., 1999. Flow and local thermal measurements in stationary and rotating cooling passages of complex geometries. Ph.D. thesis, Department of Mechanical Engineering, UMIST.

Lau, S.C., McMillin, R.D., Han, J.C., 1991. ASME J. Turbomachinery 113, 367–374.

Raisee, M.D., 1999. Computation of flow and heat transfer through two- and three-dimensional rib-roughened passages. Ph.D. thesis, Department of Mechanical Engineering, UMIST.

Taslim, M.E., Li, T., Kercher, D.M., 1996. ASME J. Turbomachinery 118, 20–28.

Wagner, J.H., Johnson, B.V., Hajek, T.J., 1989. Heat transfer in rotating passages with smooth walls. In: Proceedings of the International Gas Turbine Congress, ASME, Paper 89-GT-272.